Electromagnetic two-body problem: recurrent dynamics in the presence of state-dependent delay



2010 J. Phys. A: Math. Theor. 43 205103

(http://iopscience.iop.org/1751-8121/43/20/205103)

IOP PUBLISHING JOURNAL OF PHYSICS A: MATHEMATICAL AND THEORETICAL

J. Phys. A: Math. Theor. **43** (2010) 205103 (20pp) doi:10.1088/1751-8113/43/20/205103

# Electromagnetic two-body problem: recurrent dynamics in the presence of state-dependent delay

**Jayme De Luca[1], Nicola Guglielmi[2], Tony Humphries[3] and Antonio Politi[4]**

[1] Departamento de Física, Universidade Federal de São Carlos, Caixa Postal 676, São Carlos, São Paulo 13565-905, Brazil
[2] Dipartimento di Matematica Pura ed Applicata, Università degli Studi di L'Aquila, I-67010, L'Aquila, Italy
[3] Department of Mathematics and Statistics, McGill University, Montreal, Quebec H3A 2K6, Canada
[4] Istituto dei Sistemi Complessi, CNR Via Madonna del Piano 10–Sesto, Fiorentino I-50019, Italy

E-mail: deluca@df.ufscar.br

Received 9 October 2009, in final form 29 March 2010
Published 30 April 2010
Online at stacks.iop.org/JPhysA/43/205103

**Abstract**

We study the electromagnetic two-body problem of classical electrodynamics as a prototype dynamical system with state-dependent delays. The equations of motion are analysed with reference to motion along a straight line in the presence of an electrostatic field. We consider the general electromagnetic equations of motion for point charges with advanced and retarded interactions and study two limits, (a) retarded-only interactions (Dirac electrodynamics) and (b) half-retarded plus half-advanced interactions (Wheeler–Feynman electrodynamics). A fixed point is created where the electrostatic field balances the Coulombian attraction, and we use local analysis near this fixed point to derive necessary conditions for a Hopf bifurcation. In case (a), we study a Hopf bifurcation about an unphysical fixed point and find that it is subcritical. In case (b), there is a Hopf bifurcation about a physical fixed point and we study several families of periodic orbits near this point. The bifurcating periodic orbits are illustrated and simulated numerically, by introducing a surrogate dynamical system into the numerical analysis which transforms future data into past data by exploiting the periodicity, thus obtaining systems with only delays.

PACS numbers: 05.45.−a, 02.30.Ks, 03.50.De, 41.60.−m

(Some figures in this article are in colour only in the electronic version)

  

## 1. Introduction

In recent years, interest in dynamical systems with state-dependent delays has grown considerably despite the difficulties due to the infinite dimensionality of the phase space, and a lack of a systematic theory for such problems. Examples of such systems can be found in contexts as different as population dynamics [1], neural networks [2] and secure communication [3]. In this paper, we investigate the dynamics of two point charges as described by classical electrodynamics [4, 5]—a fundamental Physics model that belongs to this class of systems. So far, because of its mathematical complexity, this problem has mostly been tackled by invoking approximations whose reliability is difficult to control. We will consider the full problem in a one-dimensional setup, with the two particles moving along a straight line in the presence of an external electrostatic field.

Besides delayed and advanced interactions, the electromagnetic equations of motion of charged particles have a further peculiarity, namely the presence of a third-order time derivative which is responsible for seemingly paradoxical results. An example was discovered by Eliezer [6] for the motion of a single electron in the Coulombian field of an infinitely massive proton: the electron is only attracted until the third-derivative term causes the acceleration to change the sign, and the electron is *always* repelled [6]. This avoided collision is called Eliezer's theorem and the fact that the electron always escapes collision suggests that the underlying physical model is somehow over-simplified. In fact, in [7], it was suggested that some potentially complex dynamics is lost in the infinite-mass limit, which removes the delay from the equations of motion. One of the motivations of this paper is to study the effect of finite masses in the case of two particles moving along the same straight line. Since in 1D there are no centrifugal forces that can sustain a bounded motion, we introduce an external electrostatic field to provide such a force.

We start from the general equations of motion [4] for charged particles with retarded and advanced interactions, and consider the particular cases of (a) Dirac electrodynamics with retarded-only interactions [5] and (b) Wheeler–Feynman electrodynamics [8] with half-retarded plus half-advanced interactions, a case of physical interest where the self-interaction vanishes. The external field produces a fixed point by balancing the Coulombian attraction and we study the conditions for a Hopf bifurcation in both cases.

One of the differences with respect to a Coulombian two-body problem is an exponential correction to the force field (see (2)). In case (a), we show that for the correct sign of the exponent (which is absent in the Newtonian formulation) no Hopf bifurcation occurs, but upon changing the sign of the exponent, a family of periodic orbits may appear/disappear in a subcritical Hopf bifurcation. As a result, it turns out that a family of periodic orbits exists, although this happens only for the *wrong* sign of the exponent. In spite of the unphysical character of this solution, we have nevertheless explored the corresponding periodic orbits, as an example of state-dependent delay dynamics with electromagnetic-like difficulties and correct Newtonian limit. Moreover, the delicate dependence on the precise force law is a warning for future studies of a realistic version of Eliezer's theorem with a finite protonic mass, i.e. velocity-dependent forces should be carefully taken into account, if the electron changes direction to avoid a collision.

In case (b), families of periodic orbits for the full nonlinear equations are found in the vicinity of the fixed point for the correct sign of the exponent, near to the critical parameter values found from the linear analysis, and so we can conclude that the Wheeler–Feynman electrodynamics undergoes a physical Hopf bifurcation.

In both cases we numerically study the full nonlinear equations to determine the bifurcating periodic orbits. Despite the simplicity of the physical setup, it is necessary to take some care

in the numerical analysis, starting with the choice of an appropriate numerical scheme. In particular, to avoid the known explosive instabilities of the Dirac equation [9], case (a) must be integrated backward in times. As a result, the *delay*, becomes an *advance*. Case (b), the Wheeler–Feynman electrodynamics, does not suffer from runaway instabilities and can be integrated either forward or backward in time, but the problem contains both advanced and retarded arguments in either time direction. We can study the existence of periodic orbits of advanced and advanced-retarded equations by subtracting multiples of the period from the advanced arguments to transform them into retarded ones. We do this by introducing a surrogate dynamical system with an adjustable parameter that is equivalent to the original dynamics along a periodic orbit, when the parameter is equal to a multiple of the period. The equations of motion are then integrated with RADAR5, an integrator for differential-algebraic equations with state-dependent delay [10].

In case (a), we find that the time-reversed surrogate dynamical system has a stable invariant set in the form of a paraboloid with the fixed point as its base. The system undergoes a subcritical Hopf bifurcation from the fixed point on this paraboloid, and on the correct side of the critical parameter value there is a unique unstable orbit. This periodic orbit of the Dirac equations is determined by following orbits on the paraboloid with smaller and larger amplitudes that spiral away from the periodic orbit and using a bisection technique. Case (b) is harder to treat numerically because the Wheeler–Feynman equations are reversible and do not possess asymptotically stable limit sets near the fixed points. Nevertheless we find two families of periodic orbits for the full nonlinear equations including one where the delay and advance time for small amplitude orbits is exactly half a period, and another where the heavier particle is at rest, while the lighter particle oscillates, which we call frozen proton orbits.

In summary, in the next section, we introduce the model and the corresponding notations, and show the existence of two fixed point solutions, one physical and other unphysical, while section 3 is devoted to the linear stability analysis of the general model. In section 4, the linear stability analysis is applied to the case of the Dirac equations to show that there is no Hopf bifurcation form the physical point, but that there is a Hopf bifurcation from the unphysical point for arbitrary mass ratios. Section 5 is devoted to a numerical study of this Hopf bifurcation, which is revealed to be subcritical, and the resulting branch of periodic orbits is studied. In section 6 the linear stability analysis is applied to the Wheeler–Feynman equations of motion, revealing the possibility of Hopf bifurcations for both the physical and unphysical point. In section 7 the Hopf bifurcation from the physical point for the Wheeler–Feynman equations is studied using numerical simulations. In the last section we summarize our results and comment on future perspectives.

## 2. The model

We introduce the equations for straight line motion, by referring to a unit system where the speed of light is $c = 1$, the electronic mass is $m_2 = 1$ and the electronic charge is $e_2 = -1$. The two point particles have charges $e_1 = 1$ and $e_2 = -1$ and masses $m_1$ and $m_2$, respectively. Assuming particle 2 to be on the left-hand side along the line of motion, we introduce world-lines parametrized by the proper time $\tau_k$ in a reduced Minkowski space $\mathbf{x}_k(\tau_k) = (t_k(\tau_k), x_k(\tau_k))$ where $k \in (1, 2)$ and $x_k$ is the position along the line (with a negative sign for particle 1, in order to obtain more symmetric equations). Once the Minkowski velocity is a time-like unit vector, it is convenient to parametrize it by the velocity angle $\phi_k$:

$$\left(\frac{\mathrm{d}t_k}{\mathrm{d}\tau_k}, \frac{\mathrm{d}x_k}{\mathrm{d}\tau_k}\right) = (\cosh(\phi_k), \sinh(\phi_k)). \tag{1}$$

The electrodynamics of point charges was derived by Eliezer [4] generalizing Dirac's theory [5]. In Eliezer's theory the particle fields are defined by the most general solution of Maxwell's equations, a solution containing retarded and advanced fields with a constant composition parameter $\chi$. For the special case of collinear motion, the magnetic field of each particle vanishes along the line of motion and the electric-field has a simple form with the familiar Coulombian limit (see [11]). By expressing the equations of motion [4] using the velocity angle (1), we find (see [11]) that

$$m_k \frac{\mathrm{d}\phi_k}{\mathrm{d}\tau_k} - \frac{2}{3}\chi \frac{\mathrm{d}^2\phi_k}{\mathrm{d}\tau_k^2} = (1+\chi)\frac{\exp\left(2\phi_j^-\right)}{2r_{kj}^2(-)} + (1-\chi)\frac{\exp\left(-2\phi_j^+\right)}{2r_{kj}^2(+)} - \varepsilon_k, \tag{2}$$

where $k = 1, 2$ and $j = 3 - k$, and $\varepsilon_k$ is the external electric field at position $x_k$. Unlike the case of three-dimensional motion, the electric field evaluated along the line of motion depends only on the retarded and advanced velocities *and not* on the retarded and advanced accelerations. This simplification yields delay equations rather than neutral-delay equations. The presence of the exponential terms $\exp\left(2\phi_j^-\right)$ and $\exp\left(-2\phi_j^+\right)$ is one of the key differences mentioned in the introduction with respect to a Newtonian model. The electric field $\varepsilon_k$ is assumed to depend linearly on the position (see (5) and (7) for a more precise definition). This is the minimal assumption which breaks the translational invariance and thus avoids the onset of secular terms. Finally, equation (2) uses the position of the other particle at an advanced and a retarded position, each defined by a state-dependent condition $r_{kj}(\pm)$, as follows. The state-dependent advanced-light-cone distance between the two particles, $r_{kj}(+)$ is defined by

$$r_{kj}(+) \equiv t_j^+ - t_k = \left|x_k(t_k) + x_j\left(t_j^+\right)\right|, \tag{3}$$

where $t_j^+$ is the advanced time of particle $j$ and, because of the introduction of a reversed coordinate for particle 1, the distance is expressed as the *sum* of the coordinates. The state-dependent retarded-light-cone distance between the particles, $r_{kj}(-)$, is defined by

$$r_{kj}(-) \equiv t_k - t_j^- = \left|x_k(t_k) + x_j\left(t_j^-\right)\right|, \tag{4}$$

where $t_j^-$ is the retarded time of particle $j$ and again because of the reversed coordinate for particle 1, the distance is expressed as the sum of the coordinates. The equations are referred to as implicitly state-dependent, since the advanced and retarded times $t_j^\pm$ depend on the state of the system $x_j\left(t_j^\pm\right)$ at the advanced/retarded time $t_j^\pm$, and (3) and (4) must be solved implicitly for each $t_k$ to find the corresponding $t_j^\pm$. Implicitly state-dependent problems are much more difficult to tackle than the more commonly considered explicitly state-dependent problems, where the delayed time $t_j^-$ would be a function of the current time $t_k$ and current state $x_j(t_k)$ only.

In the small $\phi_k$ limit, the force in equation (2) reduces to the standard Coulombian attraction (after undoing the reversed-coordinate transformation). More generally, the term $\exp\left(2\phi_j^-\right)$ corresponds to the usual denominator of the Lienard–Wiechert fields [7] expressed in velocity-angle variables. Because of this exponential, at large velocities the equation is very different from the Galilei-invariant Coulomb problem with self-interaction. Because of the complexity of the problem, we shall not study solutions with very large velocity, even though these would be interesting candidates for identifying stable time-dependent orbits.

The equations of motion (1)–(4) *formally* have two families of fixed points, both with $\phi_1 = \phi_2 = 0$, and the electric fields having the same value $\varepsilon_o \equiv 1\big/\left(4r_o^2\right)$ where $r_o > 0$ and (i) $x_1 + x_2 = 2r_o$ and (ii) $x_1 + x_2 = -2r_o$. Point (i) violates the assumption that particle 2 is on the left-hand side and is artificial, since it corresponds to the wrong sign of both the past and the future velocities in the Lienard–Wiechert field of the other particle (right-hand side of equation (2)). This term is responsible for the only difference between the dynamics

about the two fixed points. In a simplified model containing only the Coulombian interparticle interaction, these points would be equivalent, so that (i) and (ii) are called the unphysical and the physical point, respectively.

## 3. Linear stability analysis

We will study period solutions of the equations of motion (1)–(4), by finding Hopf bifurcations from the fixed points. To do this we linearize the equations of motion about the equilibrium states, and identify parameter values for which the fixed points are linear centers. Using the evolution parameter $t = t_1 = t_2$ and expanding the $\cosh(\phi_k)$ on the right-hand side of equation (1) show that up to $\mathcal{O}(\phi_k^2)$ we have $t = \tau_1 = \tau_2$. We further shift the origin of each particle's coordinates to that of the fixed point of interest and define the new coordinates as

$$x_k = \pm r_o + r_o y_k, \tag{5}$$

where $r_o > 0$, so that the linearization of equation (1) yields

$$\phi_k = r_o \dot{y}_k. \tag{6}$$

For the electrostatic field we assume the linear spatial dependence

$$\varepsilon_k = \varepsilon_o(1 + \alpha_k y_k), \tag{7}$$

where $\varepsilon_o \equiv 1/(4r_o^2)$, which removes the translational invariance from the system, and the two families of fixed points of the system reduce to two isolated fixed points, (i) the unphysical point, $x_k = r_o$ and $\phi_k = y_k = 0$, and (ii) the physical point, $x_k = -r_o$ and $\phi_k = y_k = 0$, for both of which the electrostatic force and the interparticle attraction are in balance.

The linearly varying electric field also removes the exact symmetry of the equations of motion (1)–(4), defined in the case of constant electric fields by a one-parameter continuous boost symmetry $\gamma_B \equiv \cosh(\Gamma)$:

$$\begin{aligned} x_j &\to \cosh(\Gamma)x_j - \sinh(\Gamma)t_j, \\ t_j &\to \cosh(\Gamma)t_j - \sinh(\Gamma)x_j, \\ \phi_j &\to \phi_j + \Gamma, \end{aligned} \tag{8}$$

where $\Gamma$ is a real parameter (which must be the same for both particle transformations). Symmetry (8) is the Lorentz invariance of the equations of motion. Since the electric field is unchanged by this symmetry transformation, changing the electric field is an action above the symmetry transformation. This symmetry that the equations of motion are the same in two inertial frames moving at a constant speed about each other causes secular behavior in numerical simulations with constant electric fields, as the orbit travels with a small constant velocity representing the symmetry drift; thus, we consider the case where at least one $\alpha_k \neq 0$.

Linearizing the equations of motion (1)–(4) together with (5)–(7), the linear correction to the delay gives only second-order contributions to the tangent dynamics, so that we can approximate the delay with $2r_o$, i.e. the delay is constant. Substitution of equation (6) into equation (2) yields the linearized equations of motion:

$$\begin{aligned} -\frac{2}{3}r_o\chi\dddot{y}_k + m_k r_o \ddot{y}_k = {} & \frac{(1+\chi)}{8r_o^2}[\mp y_k \mp y_j(t-2r_o) + 2r_o\dot{y}_j(t-2r_o)] \\ & + \frac{(1-\chi)}{8r_o^2}[\mp y_k \mp y_j(t+2r_o) - 2r_o\dot{y}_j(t+2r_o)] - \frac{\alpha_k}{4r_o^2}y_k, \end{aligned} \tag{9}$$

where $k = 1, 2$ and $j = 3 - k$. In order to obtain a unified treatment of the general case, we replace $\alpha_k$ with $\psi_k$ according to the following relation:

$$(\alpha_k \pm 1) \equiv -(1 - \psi_k), \qquad k = 1, 2. \tag{10}$$

Now, we search for harmonic linear modes of equation (9) by making the ansatz $y_k = \mathrm{Re}(z_k)$ where $z_k = A_k \exp(\mathrm{i}\omega t)$. Here, and throughout, $\mathrm{i} \equiv \sqrt{-1}$. It is also convenient to introduce the parameter $\sigma \equiv 2r_o\omega$ measuring the phase shift during the light-cone time-lag $2r_o$. From equation (9), we obtain equations for the complex numbers $A_k$:

$$\begin{pmatrix} B_1 & B_\pm \\ B_\pm & B_2 \end{pmatrix} \begin{pmatrix} A_1 \\ A_2 \end{pmatrix} = \begin{pmatrix} 0 \\ 0 \end{pmatrix}, \tag{11}$$

where

$$\begin{aligned} B_\pm &\equiv \sigma \sin(\sigma) \mp \cos(\sigma) + \mathrm{i}\chi(\sigma \cos(\sigma) \pm \sin(\sigma)), \\ B_k &\equiv \left(1 - \psi_k + m_k r_o \sigma^2 - \frac{\mathrm{i}\chi\sigma^3}{3}\right), \qquad k = 1, 2. \end{aligned} \tag{12}$$

Here we consider two cases of equation (2): (a) $\chi \neq 0$, including the case $\chi = 1$ which represents the Dirac theory [5] with retarded fields. For low-velocity initial conditions, equation (2) with $\chi = 1$ presents an exponential runaway instability that forces us to integrate it backward [11]. Along a backward integration the delay becomes an advance, which makes integration impossible. Assuming the orbit to be periodic, we introduce a method to re-access this retarded information from future data using the periodic property (we recall that future data *are known* along the backward integration). (b) $\chi = 0$ which represents the Wheeler–Feynman electrodynamics [8]. In this case the forward integration needs future data, and we again use the periodic property to read future data from the interpolated past using a period-$T$ shift. In all cases treated here the method only works for periodic orbits by reading the future data from the interpolated past via the period shift. In the following we discuss the two cases separately.

## 4. The mixed case (a)

We first consider the non time-symmetric case $\chi \neq 0$. Equating the determinant of equation (11) to zero, we obtain one equation for the real part and one for the imaginary part, respectively. The imaginary part yields

$$(m_1 + m_2) r_o \sigma^2 = \psi_1 + \psi_2 + a(\sigma)\sigma^2, \tag{13}$$

where $a(\sigma)$ is defined as

$$a(\sigma) = \frac{6(\pm\cos(\sigma) - \sigma \sin(\sigma))(\pm\sin(\sigma) + \sigma \cos(\sigma)) - 2\sigma^3}{\sigma^5}. \tag{14}$$

Using (13), the real part of the determinant can be rearranged into a quadratic equation for the $\psi_k$ variables:

$$\theta^2 + (m_2 - m_1) a \sigma^2 \theta + C = 0, \tag{15}$$

where

$$\theta \equiv m_2\psi_1 - m_1\psi_2, \tag{16}$$

and $C$ is defined by

$$\begin{aligned} C = (m_1 + m_2)^2 \Bigg[ &-1 - a\sigma^2 + (\pm\cos(\sigma) - \sigma \sin(\sigma))^2 \\ &- \chi^2(\pm\sin(\sigma) + \sigma \cos(\sigma))^2 + \frac{\chi^2\sigma^6}{9} \Bigg] - m_1 m_2 a^2 \sigma^4. \end{aligned} \tag{17}$$

Since equations (13) and (15) are both even in $\sigma$, it is sufficient to consider $\sigma = 2r_o\omega > 0$ in what follows. The corresponding solutions with $\sigma < 0$ will simply have reversed direction of rotation.

The discriminant $D$ of the quadratic equation (15) is

$$D(\sigma) = 4(m_1+m_2)^2\left[(\pm\cos(\sigma) - \sigma\sin(\sigma))^2 + \frac{\chi^2\sigma^6}{9}\right] \times \left[\frac{9}{\sigma^6}(\pm\sin(\sigma) + \sigma\cos(\sigma))^2 - 1\right]. \tag{18}$$

For the physical fixed point (ii), $D(\sigma) < 0$ for all $\sigma > 0$ and so there are no real solutions of equation (15), and so no periodic orbits bifurcating from this fixed point. On the other hand, in the case of the unphysical point (i), $D(\sigma) > 0$ for all $\sigma \in (0, \sigma^*)$ where $\sigma^* \approx 1.494\,033$ solves

$$9(\sin(\sigma) + \sigma\cos(\sigma))^2 - \sigma^6 = 0, \tag{19}$$

so there always exists a Hopf bifurcation for *any* mass ratio in the case of the unphysical point (i). In principle one can choose an arbitrary $\chi \neq 0$, $\sigma \in (0, \sigma^*)$ and $M \equiv m_1 + m_2$ and find solutions for $\alpha$ from equation (15).

In the Dirac case, $\chi = 1$, for fixed point (i) with $\alpha = 0$ in the large-$M$ limit, there exists an asymptotic root of equations (9) that is given by

$$\sigma \simeq \sqrt{12\mu/M}, \qquad r_o \simeq M/(12\mu^2), \tag{20}$$

where $\mu = m_1m_2/M$, and the critical period $T_c = 2\pi/\omega_c$ defined by $\sigma = 2\omega_c r_o$ is

$$T_c = \frac{\pi}{\sqrt{108}}\frac{M^{3/2}}{\mu^{5/2}}. \tag{21}$$

In the infinite-$M$ limit equation (20) predicts an infinite separation and a vanishing oscillation frequency.

## 5. Numerical integration of the Dirac case (a)

We consider the unphysical point (i) in the Dirac case $\chi = 1$, Now choose masses $m_1 \neq m_2$ and $\sigma \in (0, \sigma^*)$, and solve equation (15) to find $\theta$. In the case $\alpha_1 = \alpha_2 = \alpha$, equation (16) implies that $\alpha = -2+\theta/(m_2-m_1)$. Equation (13) can be solved to find $r_o$, while $\varepsilon_o$, $\omega_c$ and $T_c$ follow from $\varepsilon_o = 1\big/\left(4r_o^2\right)$, $\sigma = 2r_o\omega_c$ and $T_c = 2\pi/\omega_c$. Hence we determine the bifurcation point from the linearized equations of motion (7), (9) and (10).

To solve the nonlinear equations of motion (1)–(4), we parametrize the solution of equations (1)–(4) by $t = t_1(\tau_1) = t_2(\tau_2)$, whereby each proper time is a function of the common particle time and $\tau_k$ is a monotonic function of $t$ with derivative defined by equation (1), i.e.

$$\frac{\mathrm{d}\tau_k}{\mathrm{d}t} = \frac{1}{\cosh(\phi_k)}. \tag{22}$$

Equation (22), complemented by equations (1)–(4) and by a suitable portion of the history, defines a Cauchy problem for a state-dependent delay equation. For low-velocity initial conditions, equation (2) presents an exponential runaway instability that forces us to integrate it backward [11]. When integrating backward, it is necessary to use the future to construct the past, which is problematic because the algebraic conditions (1) need past data. However, this difficulty can be overcome along a periodic orbit by shifting a past state forward by one

period so that it becomes a future state so that along the periodic motion equation (4) becomes equivalent to

$$t_j^- = t - r_{kj} + T = \left|x_k(t) + x_j\left(t_j^-\right)\right|. \tag{23}$$

Noting that $T_c = 4\pi r_o/\sigma > 8r_o$, and that in the limit of small amplitude periodic orbits (close to the bifurcation point) $r_{kj}$ is equal to $2r_o$, equation (23) is guaranteed to produce an advanced argument for such orbits. Should the period and amplitude vary as we vary other parameters until $T < r_{kj}$, then (23) would no longer produce an advanced argument, but this could be remedied by replacing $T$ by $nT$ in (23) for a suitable integer $n$, although in practice we did not need to do this for the Dirac problem.

By replacing equation (4) with equation (23), we obtain a surrogate dynamical system with an adjustable parameter $T$. In this way we have a well-posed Cauchy problem with suitable initial data. In the following we study this surrogate dynamical system defined by equations (1), (2) and (23) near the critical point. It is easy to verify that if the surrogate system has a periodic orbit of period $T$, this is also an orbit of the original physical problem.

The nonlinear equations of motion (1)–(4), (22) and (23) are then integrated numerically with RADAR5, an integrator for differential-algebraic equations with state-dependent delay [10], using the just determined parameters $T_c$ and $\varepsilon_o$ while $\alpha$ is taken to be close to its value at the Hopf bifurcation. We use initial conditions $y_k = A_k \cos(\omega t + \beta_k)$, with $\beta_1 = 0$, $A_1$ set equal to some preassigned small value, $A_2/A_1$ and $\beta_2$ in agreement with the critical behavior defined by equation (11) and $\omega$ equal to or slightly shifted with respect to criticality to correspond to the same period $T \approx T_c$ set in the surrogate system. The parameter $T$ in (23) is then the only parameter which is varied during the actual numerical integration. Every $n$ time units $T$ is adjusted to agree with the numerically measured period of the oscillation. If the amplitude of the oscillation remains constant, these adjustments ensure that the period of the resulting solution equals $T$ itself.

Performing these computations we find that solutions for the time reversed surrogate system rapidly converge to an invariant paraboloid which has a fixed point as its base. On this surface there is a unique unstable periodic orbit for each $\alpha < \alpha^*$ (where $\alpha^*$ is the value of $\alpha$ at the bifurcation), and no other periodic orbits were found. On the paraboloid, solutions inside the periodic orbit spiral very slowly into the fixed point, while solutions outside the periodic orbit spiral away. For $\alpha > \alpha^*$ the invariant paraboloid persists and is still stable for the time reversed surrogate system, but in this case there are no periodic orbits on or off the paraboloid, and orbits on the paraboloid spiral away from the fixed point.

Despite the infinite dimensionality of the phase space, the unstable periodic orbits lie on a stable invariant paraboloid of the backward dynamics, and so can be found by identifying an initial condition leading to a solution of the surrogate system that spirals into the fixed point, and another initial condition leading to a solution that spirals out. Varying the initial condition between these values, using the bisection algorithm, the periodic orbit is found, and the entire numerical procedure works well.

As an example, in figure 1 we plot a phase portrait with 11 orbits of the time reversed surrogate system for $m_1 = 1$, $m_2 = 250$, $r_o = 27.946\,237$. For these parameter values the linearization with $\sigma = 0.2$ indicates a Hopf bifurcation at $\alpha^* = 0.115\,232$ with the zero amplitude periodic orbit thus created having period $T_c = 1755.913\,842$. The numerically computed trajectories shown in figure 1 were computed with $\alpha = 0.113 < \alpha^*$, and show a periodic orbit (thin line) whose period is $T = 1761.874\,955$. The ten other orbits (thick lines) are not periodic, but clearly lie on an invariant surface in the infinite dimensional flow, which has the form of a paraboloid. This invariant surface is attractive in the time-reversed surrogate system, and so can be found by taking arbitrary nearby initial conditions and integrating

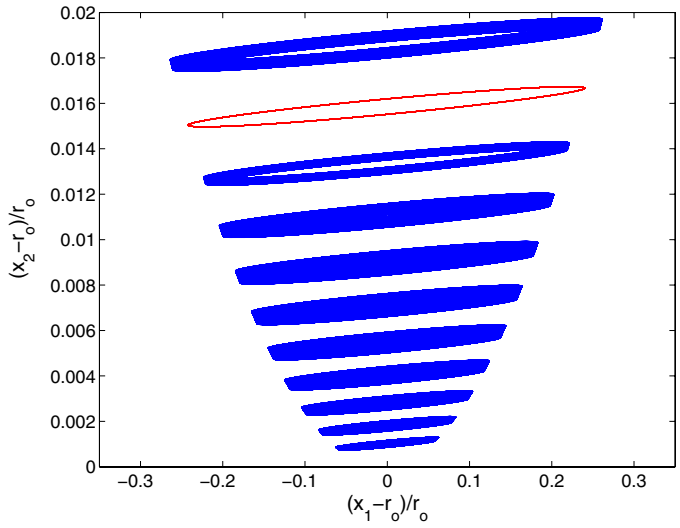


**Figure 1.** Orbits with $m_1 = 1$, $m_2 = 250$, $r_o = 27.946\,237$, $\alpha = 0.113$ showing the periodic orbit (thin line) and ten other spiralling orbits of the time reversed surrogate system.

until the end of the initial transient dynamics as the solution converges to the paraboloid. Although difficult to see from the figure, the orbits below the period solution are spiralling toward the fixed point, while the orbit above is spiralling away. Of course, for non-periodic orbits, equation (23) means that the dynamics of the surrogate system is not equivalent to that of the original state-dependent delay equations, but nevertheless we expect such an invariant manifold to also exist for the original system.

Next, we consider the evolution of the periodic orbit as the electric field parameter $\alpha$ is varied. We again consider $m_1 = 1$, $m_2 = 250$ and $r_o = 27.946\,237$, and then vary $\alpha$ between the critical value $\alpha^* = 0.115\,2323$ and $\alpha^* - 0.005$. In figure 2 we see that the amplitude of the periodic orbit varies proportional to $(\alpha^* - \alpha)^{1/2}$ with the amplitude of the $x_1$ oscillation already growing to approximately $0.36r_o$ (that is 0.18 times the rest separation between the particles) when $\alpha = \alpha^* - 0.005$. In figure 3 we see that the period of the periodic orbit varies linearly but slowly with $\alpha$, varying by less than one percent over the same range of values of $\alpha$. The square root variation of the amplitude, and linear variation of the period are characteristic of Hopf bifurcations, and we conclude that a Hopf bifurcation occurs in the time-reversed surrogate system, and hence in the original state-dependent DDE. For the time-reversed system, the bifurcation is subcritical since the fixed point is stable for values of $\alpha$ for which the periodic orbit exists, but unstable in the parameter regime for which periodic orbits do not exist.

In figure 4 we show the evolution of the periodic orbits as $\alpha$ is varied by plotting 20 periodic orbits for different values of $\alpha$. Away from the critical value $\alpha^*$, the orbits have increasing amplitude for the oscillation of the light particle $m_1$ about the rest value $r_o$, while the heavy particle $m_2$ is virtually at rest, but is perturbed away from its equilibrium value. This perturbation of the heavy particle from equilibrium is caused by the periodic motion of the light particle $m_1$, which over one period exerts an average force on the heavy particle $m_2$ which is greater than if $m_1$ were at rest, effectively moving the equilibrium point for the heavy particle. For these large amplitude solutions the periodic orbit found does not enclose the fixed point $x_1 = x_2 = r_o$ and so we are far from the linear case for which periodic orbits have the form $x_k = r_o + r_o A_k \exp(\mathrm{i}\omega t)$ and are thus necessary concentric about $x_1 = x_2 = r_o$. The

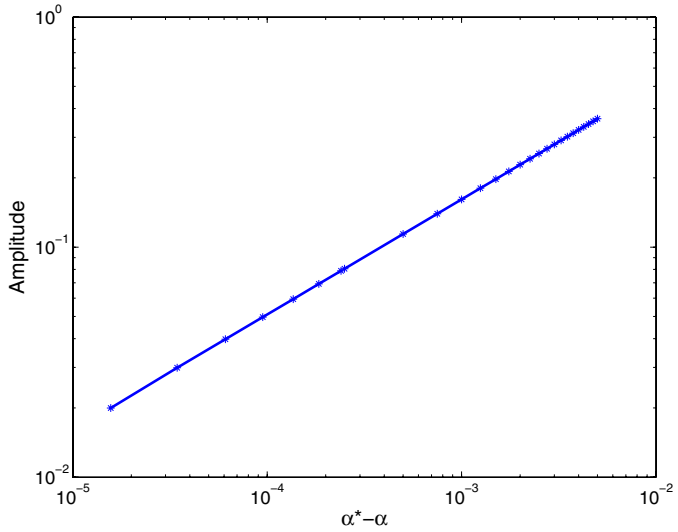


**Figure 2.** Bifurcation diagram showing the amplitude of periodic orbits with $m_1 = 1$, $m_2 = 250$, $r_o = 27.946\,237$, $\alpha^* = 0.115\,232$ and $T_c = 1755.913\,842$. Amplitude is measured using the light particle $x_1$ and scaling by $r_o$, so amplitude $= \frac{1}{r_o}(\max_{\tau_1}\{x_1(\tau_1)\} - \min_{\tau_1}\{x_1(\tau_1)\})$. A log-scale is used to show that the amplitude of the periodic orbit varies: amplitude $\propto (\alpha^* - \alpha)^{1/2}$.

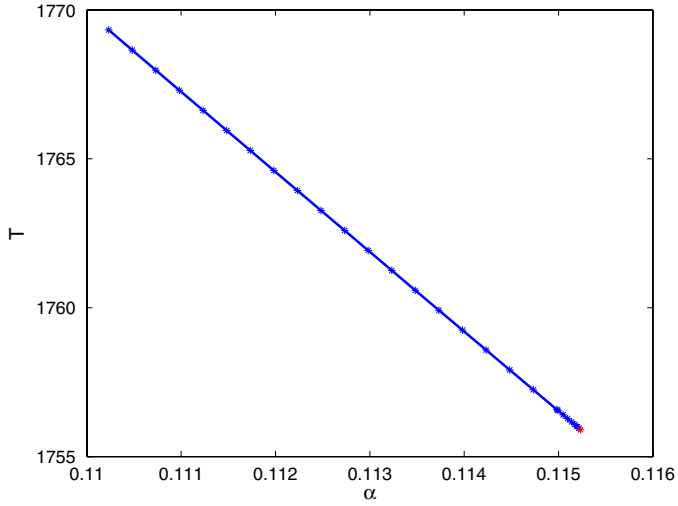


**Figure 3.** Bifurcation diagram showing period of periodic orbits with $m_1 = 1$, $m_2 = 250$, $r_o = 27.946\,237$, $\alpha^* = 0.115\,232$ and critical period $T_c = 1755.913\,842$.

linearized dynamics, which treat the delays as constant, and so strictly are only valid in the limit of infinitesimally small oscillations, however do provide a reasonable approximation to the dynamics of the full system in the case of orbits of small amplitude.

Similar dynamics can be observed with other mass ratios, though when $m_2/m_1$ is very large, the oscillations of the heavy particle are barely discernable, and in figure 5 a branch of periodic orbits is shown for $m_1 = 1$ and $m_2 = 1836$.

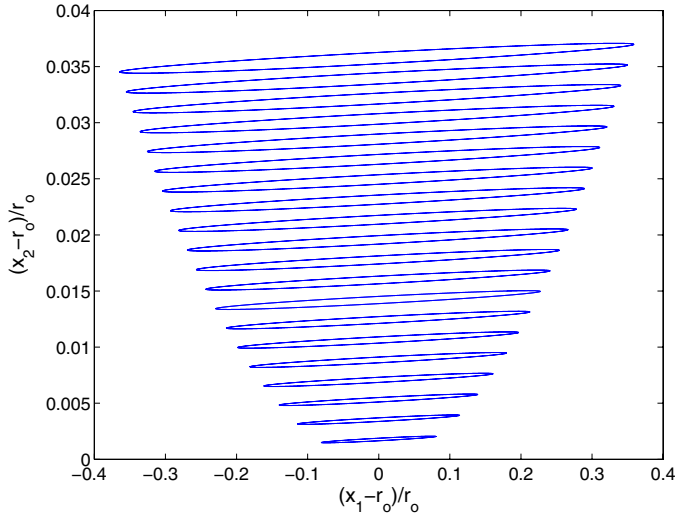


**Figure 4.** Twenty periodic orbits with $m_1 = 1$, $m_2 = 250$, $r_o = 27.946\,237$ and different values of $\alpha$ for each orbit between 0.110 232 (the largest orbit) and 0.114 982 (the smallest orbit) smaller than the critical value $\alpha^* = 0.115\,2323$.

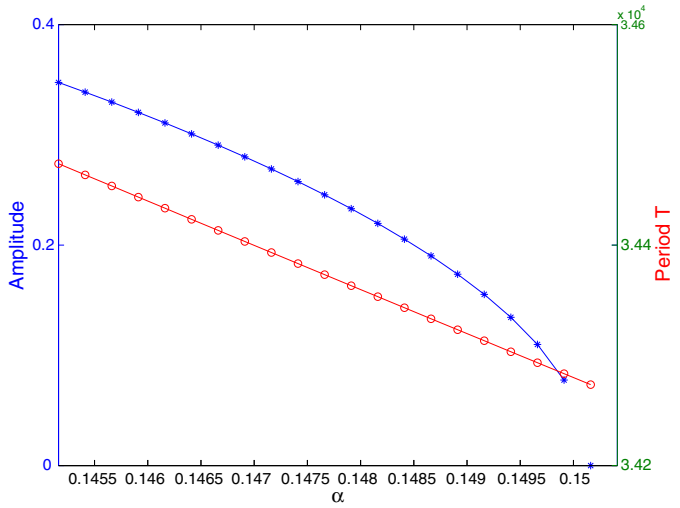


**Figure 5.** Amplitude (varying quadratically) and period (varying linearly) of branch of periodic solutions as $\alpha$ is varied with $m_1 = 1$, $m_2 = 1836$, $r_o = 204.5541$, $\varepsilon_o = 5.974\,8034 \times 10^{-6}$ and $\alpha^* = 0.150\,1618$.

## 6. The Wheeler–Feynman case (b)

In the case $\chi = 0$ the equation of motion is of mixed type, i.e.

$$m_k \frac{\mathrm{d}\phi_k}{\mathrm{d}\tau_k} = \frac{\exp\left(2\phi_j^-\right)}{2r_{kj}^2(-)} + \frac{\exp\left(-2\phi_j^+\right)}{2r_{kj}^2(+)} - \varepsilon_k. \tag{24}$$

Equation of motion (24) for particle $k$ uses the other particle's position and velocity at the advanced time $t_j^+$ defined by the state-dependent condition (3) and the other particle's position and velocity at the retarded time $t_j^-$ defined by the state-dependent condition (4).

With (5)–(7) the fixed points are the same as for the $\chi \neq 0$ case, (i) the unphysical point, $x_k = r_o$ and $\phi_k = y_k = 0$, and (ii) the physical point, $x_k = -r_o$ and $\phi_k = y_k = 0$, where again $2r_o > 0$ is the separation at the fixed point. The characteristic equation (11) is real for both cases and the determinant is

$$(\mp 1 - \alpha_1 + m_1 r_o \sigma^2)(\mp 1 - \alpha_2 + m_2 r_o \sigma^2) = (\sigma \sin(\sigma) \mp \cos(\sigma))^2. \tag{25}$$

To solve equation (25) it is convenient to set $\alpha_1 = \alpha$ and $\alpha_2 = \kappa\alpha$, so that $\kappa = \alpha_2/\alpha_1$ when $\alpha_1 \neq 0$. Then equation (25) can be written as a quadratic in $\alpha$:

$$\begin{aligned} 0 = \kappa\alpha^2 + [\pm(1+\kappa) - (\kappa m_1 + m_2) r_o \sigma^2]\alpha \\ + (1 \mp m_1 r_o \sigma^2)(1 \mp m_2 r_o \sigma^2) - (\sigma \sin(\sigma) \mp \cos(\sigma))^2 \end{aligned} \tag{26}$$

with discriminant

$$d(\kappa, \sigma) = [(1-\kappa) \pm (\kappa m_1 - m_2) r_o \sigma^2]^2 + 4\kappa(\sigma \sin(\sigma) \mp \cos(\sigma))^2. \tag{27}$$

Equation (27) illustrates the first qualitative difference of the $\chi = 0$ dynamics from the $\chi \neq 0$ case considered before. Since $d(\kappa, 0) = (1+\kappa)^2$, for both the physical and nonphysical points, whenever $\kappa \neq -1$ (that is whenever $\alpha_1 \neq -\alpha_2$) the discriminant $d(\kappa, \sigma) > 0$ for all small $\sigma$ and so (26) has two solutions, and the center-manifold harmonic oscillation exists in the neighborhood of both points (i) and (ii). Similarly, whenever $\kappa m_1 \neq m_2$ we have $d(\kappa, \sigma) > 0$ for all $\sigma$ sufficiently large, and again (27) has two solutions.

Moreover, let $\Sigma = \{\sigma > 0 : (\sigma \sin(\sigma) \mp \cos(\sigma)) = 0\}$ and $\Sigma^* = \{\sigma \in \Sigma : (1-\kappa) \pm (\kappa m_1 - m_2) r_o \sigma^2 = 0\}$, and note that the points of $\Sigma$ are close to $n\pi$ for large $\sigma$. If $\kappa m_1 \neq m_2$, then $\Sigma^*$ contains at most one point which is defined by

$$r_o \sigma^2 = \frac{\pm(\kappa - 1)}{(\kappa m_1 - m_2)}.$$

This point only exists if the right-hand side is positive, and the resulting $\sigma$ is contained in $\Sigma$, so generically $\Sigma^* = \emptyset$, but the parameters can always be deliberately chosen to make $\Sigma^*$ be nonempty. On the other hand, if $m_1 = m_2$ and $\kappa = 1$, then $\Sigma^* = \Sigma$ and contains countably many points. Now, for all $\kappa > 0$, and all $\sigma > 0$ such that $\sigma \notin \Sigma^*$, we have $d(\kappa, \sigma) > 0$ and so harmonic oscillations exist for both points (i) and (ii) for any positive ratio of $\alpha_2/\alpha_1$ and any $\sigma \notin \Sigma^*$.

The exceptional set $\Sigma^*$ is also very interesting. If $\sigma \in \Sigma^*$, then the discriminant $d(\kappa, \sigma) = 0$ and the quadratic equation (26) has exactly one (repeated) root $\alpha$. Also equation (25) implies that $(\mp 1 - \alpha_k + m_k r_o \sigma^2) = 0$ for both $k = 1$ and $k = 2$ so that $B_k = B_\pm = 0$ in equation (11), and solutions for $A_k$ are arbitrary. This indicates a possible bifurcation of higher co-dimension, which we will not study here. When $\kappa > 0$ either $d(\kappa, \sigma) > 0$ or $\sigma \in \Sigma^*$, so there are no other cases to consider.

For $\kappa < 0$, first consider the case of $\kappa = -1$ when $\alpha_1 = -\alpha_2$. As noted above, $d(-1, 0) = 0$, but we may also compute $d_\sigma(\kappa, 0) = 0$ for all $\kappa$ and

$$d_{\sigma\sigma}(-1, 0) = \mp 8[M r_o \mp 1 - 2],$$

so at the unphysical point (i) $d_{\sigma\sigma}(-1, 0) > 0$ if $M r_o < 3$, while at the physical point (ii) $d_{\sigma\sigma}(-1, 0) > 0$ if $M r_o > 1$ in which case, again, $d(-1, \sigma) > 0$ for all $\sigma$ sufficiently small and, as for the cases $\kappa \neq -1$, equation (26) has two solutions, and the center-manifold harmonic oscillation exists in the neighborhood of both points (i) and (ii). Since for $\kappa < 0$ necessarily $\kappa m_1 \neq m_2$, in this case there are always solutions of equation (26) for $\sigma$ sufficiently large.

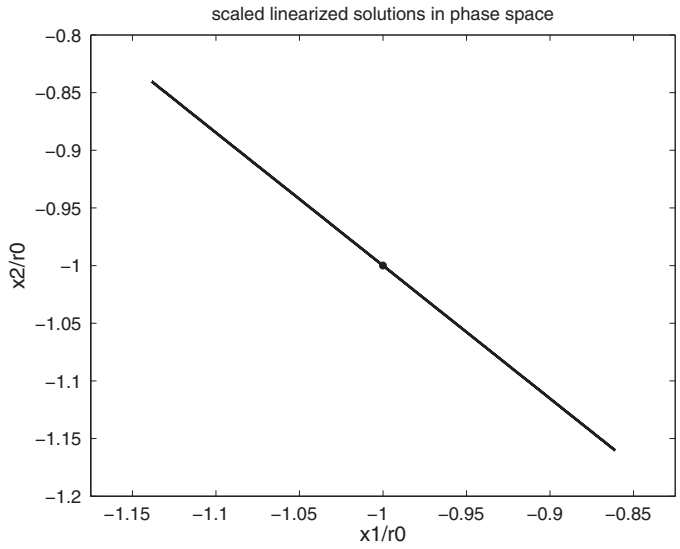


**Figure 6.** A Periodic solution of the linearized equations of motion (9) with $\chi = 0$, $m_1 = 1$, $m_2 = 2$, $r_o = 10^3$, $\varepsilon_o = 2.5 \times 10^{-7}$, $\sigma = 2.5$, $\kappa = 2$, $\alpha = 6.2502 \times 10^3$ and period $T = 5.0265 \times 10^3$ with $A2/A1 = -1.1532$.

Also when $\kappa < 0$ the set $\Sigma^* = \emptyset$ for the physical point (ii) and contains at most one point for the unphysical point (i). Nevertheless, it is possible for $d(\kappa, \sigma) < 0$ for both the physical and nonphysical point, and for $d(\kappa, \sigma) = 0$ for $\sigma \notin \Sigma^*$, when a center-manifold harmonic oscillation exists, defined by the repeated root of (26), where since $\sigma \notin \Sigma^*$, we expect a different higher co-dimension bifurcation than in the case $\sigma \in \Sigma^*$.

It is interesting to observe that at $\chi = 0$ both points (i) and (ii) have a center-manifold, but that point (ii) loses the zero-amplitude harmonic orbit for $\chi \neq 0$. Our linear stability analysis suggests that the case $\chi = 0$ is exceptional, because then the determinant of equation (11) is real and its vanishing poses a single condition, as opposed to two conditions for vanishing real and imaginary parts at any $\chi \neq 0$. The fact that the case $\chi = 0$ accepts a one-parameter family of bounded circular orbits in the 3D case [12], while no one ever found a solution for the case $\chi \neq 0$, suggests that it is the exceptional case which is the most interesting. The phenomenon of losing solutions as $\chi$ varies is a bifurcation that we shall not investigate here.

## 7. Numerical integration of the Wheeler–Feynman case (b)

In the following we search for small-amplitude periodic oscillations near the physical point (ii) and at $\chi = 0$. To do this we first choose the masses $m_1$ and $m_2$, the field ratio $\kappa$, and $r_o$. Then choosing $\sigma$ fixes $\omega$ and the period $T$ of the zero amplitude solutions, and we solve (26) to find the value of $\alpha$ for the bifurcation. Since (11) is real when $\chi = 0$, solutions of the linearized equations of motion (9) are then given by $y_k = A_k \cos(\omega t)$ where the amplitudes $A_k$ are related by

$$\begin{aligned} 0 &= B_1 A_1 + B_- A_2 \\ &= (1 - \alpha_1 + m_1 r_o \sigma^2) A_1 + (\sigma \sin(\sigma) + \cos(\sigma)) A_2, \end{aligned} \tag{28}$$

and the motions of the two particles are either in phase or anti-phase depending on $\text{sign}(B_1 B_-)$. Such a periodic solution of the linearized equations is illustrated in figure 6.

Next we consider the fully nonlinear equations of motion, equations (1), (24), (3) and (4), and parametrize the solution by $t = t_1(\tau_1) = t_2(\tau_2)$, whereby each proper time is a function of the common particle time and $\tau_k$ is a monotonic function of $t$ with derivative defined by equation (22). There is no exponential runaway of solutions for the $\chi = 0$ Wheeler–Feynman dynamics, and so equations (1), (24), (3) and (4) can be numerically integrated forward or backward in time. Equation (24) results in one advanced and one retarded argument for each particle, so four shifted arguments in total. In the case of forward integration along a periodic orbit the advanced time defined by (3) can be period-shifted to the past using

$$t_j^+ = t_k + \left|x_k(t_k) + x_j\left(t_j^+\right)\right| - T. \tag{29}$$

Since the period of the oscillation at zero amplitude is

$$T = \frac{2\pi}{\omega} = \frac{4\pi r_o}{\sigma}, \tag{30}$$

which is greater than the bifurcation delay time $2r_o$ as long as $\sigma < 2\pi$, equation (29) always gives retarded times for small amplitude orbits when $\sigma < 2\pi$. If equation (29) does not result in a delayed time, one must subtract a higher multiple of $T$. We refer to equations (1), (24), (29) and (4) as the forward surrogate dynamical system, which now has four delays. As before, if the surrogate system has a periodic orbit of period $T$, then this is a periodic orbit of the full nonlinear equations of motion. Similarly, if integrating backward in time equation (4) must be replaced by (23), resulting in a backward surrogate dynamical system (1), (24), (3) and (23) (with four 'advances').

For oscillations of small amplitude

$$x_k = -r_o + r_o A_k \cos(\omega t), \tag{31}$$

is an approximation for the periodic orbit, and can be used as an initial history to start the numerical integration, which is again performed with RADAR5 [10]. However, in contrast to the Dirac case, in the Wheeler–Feynman case of $\chi = 0$ the equation of motion (2) is reversible even with the non-constant electric field. Therefore, if a periodic orbit or other invariant set has a stable manifold, it will also have an unstable manifold. This prevents us from using the numerical approach we applied in the Dirac case, where we used the attractivity of an invariant manifold to locate the periodic orbits for the nonlinear dynamics, since such an attractive manifold cannot exist in the Wheeler–Feynman case; manifolds and orbits are either neutrally stable or have saddle structure. We illustrate this by solving the nonlinear equations of motion for the forward and backward surrogate systems starting from the initial history (31) and using the same parameters as in the linear example of figure 6.

Figure 7 shows an orbit for the forward surrogate dynamical system with initial history given by a small amplitude periodic orbit of period $T$ of the linearized equations and integrated over a time interval of $25T$. The solution of the forward surrogate system is clearly not periodic of period $T$. Although the two particles oscillate with approximately the predicted frequency, there is a gradual phase shift between the oscillations. Numerical experiments reveal that decreasing the initial amplitude of the orbit results in a slower drift, but that the drift cannot be eliminated for non-zero amplitudes for these parameter values. This suggests that there is a family of periodic orbits bifurcating from the trivial solution, in a sub- or super-critical Hopf bifurcation for some perturbed parameter values, but because of the lack of stability it is impossible to isolate this family of periodic solutions with the numerical techniques available. Nevertheless, the nonlinear orbit seen in figure 7 likely gives a good approximation to the unstable manifold of such a periodic orbit. Figure 8 is similar, except that it shows an orbit for the backward surrogate system. This also drifts away from the linear periodic orbit, but since this drift is backward in time this orbit is approaching the periodic solution of the linearized

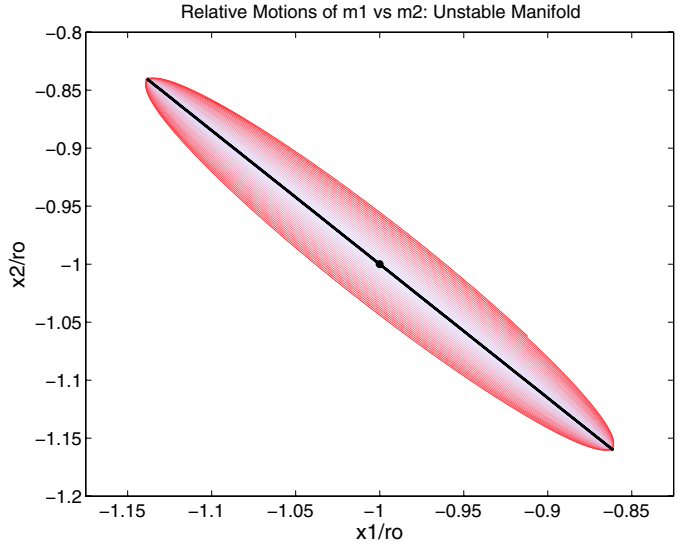


**Figure 7.** A solution of the forward surrogate dynamical system with $\chi = 0$, $m_1 = 1$, $m_2 = 2$, $r_o = 10^3$, $\varepsilon_o = 2.5 \times 10^{-7}$, $\kappa = 2$ and $\alpha = 6.2502 \times 10^3$. The periodic solution of the linearized equation (9) with $\sigma = 2.5$, period $T = 5.0265 \times 10^3$ and $A_1 = 0.139\,01$, $A_2 = -0.160\,28$ (solid straight line) is used as the initial history for the solution of the nonlinear equation (2) which is plotted progressively darkening shades (of red).

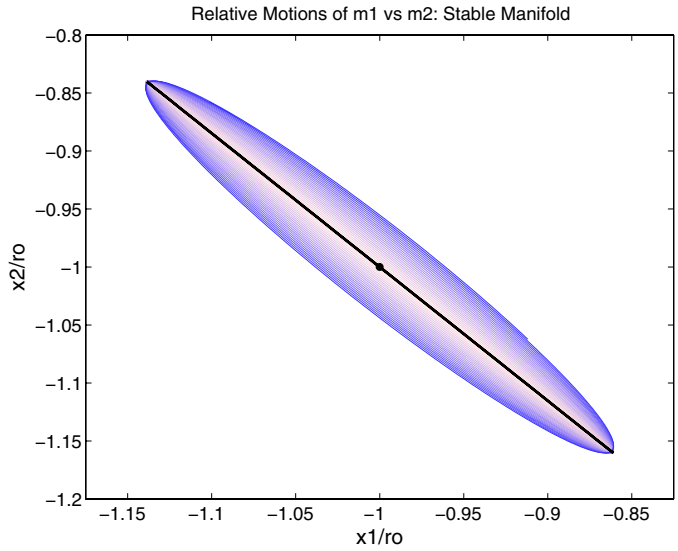


**Figure 8.** A solution of the backward surrogate dynamical system with $\chi = 0$, $m_1 = 1$, $m_2 = 2$, $r_o = 10^3$, $\varepsilon_o = 2.5 \times 10^{-7}$, $\kappa = 2$ and $\alpha = 6.2502 \times 10^3$. The periodic solution of the linearized equation (9) with $\sigma = 2.5$, period $T = 5.0265 \times 10^3$ and $A_1 = 0.139\,01$, $A_2 = -0.160\,28$ (solid straight line) is used as the initial history for the solution of the nonlinear equation (2) which is plotted in progressively darkening shades (of blue).

equations, and so gives an approximation to the stable manifold. However, the linear periodic orbit is not a solution of the nonlinear equations, so the nonlinear solution after approaching this orbit will drift away from it along the orbit plotted in figure 7.

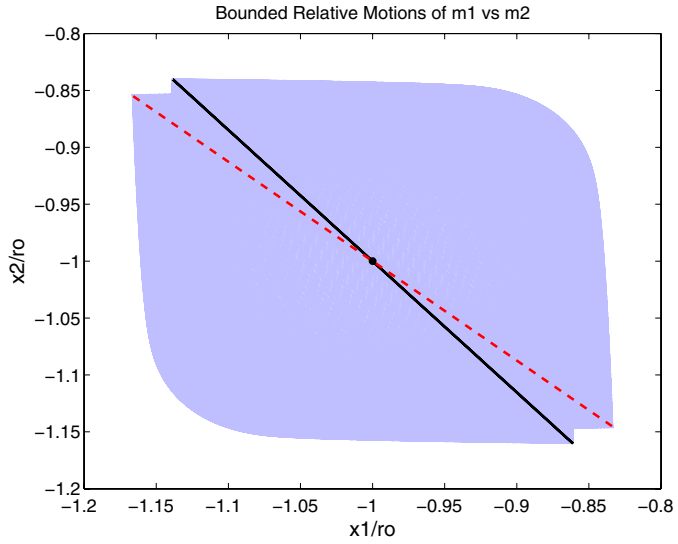


**Figure 9.** A solution (plotted in gray) of the forward surrogate dynamical system with $\chi = 0$, $m_1 = 1$, $m_2 = 2$, $r_o = 10^3$, $\varepsilon_o = 2.5 \times 10^{-7}$, $\kappa = 2$ and $\alpha = 6.2502 \times 10^3$. The periodic solution of the linearized equation (9) with $\sigma = 2.5$, period $T = 5.0265 \times 10^3$ and $A_1 = 0.139\,01$, $A_2 = -0.160\,28$ (shown in black) is used as the initial history for the solution of the nonlinear equation (2) which is plotted over a time interval of $600T$.

Although the solutions of the forward and backward surrogate systems drift away from the periodic solution of the linearized equations, unlike the Dirac case, there is no runaway instability in the Wheeler–Feynman case and the orbits of the surrogate dynamical system remain bounded for all time. We plot one such orbit in figure 9 over a time interval of $600T$. The oscillations of the two particles, which start in the phase (along the solid line in the figure) persist over this time interval and return into the phase (dashed line in the figure). Integrating another $600T$ time units, the system returns to the original configuration. This memory of the initial conditions is another reason why our approach from the previous section of integrating toward the periodic orbit will fail; not only will the periodic orbit have an unstable manifold if it has a stable manifold, but any error between the initial conditions and the periodic orbit are retained rather than converging to zero through the computation.

For general values of the parameters, we would like to vary $\alpha$ slightly from the bifurcation value and find a bifurcating family of periodic orbits for the full nonlinear equations, but as illustrated above, this approach will not work using RADAR5 because of the lack of stability of the orbits. The lack of stability would not be a problem if we had access to a boundary value problem solver that could directly find the periodic orbits of an implicitly state-dependent advanced-retarded system, but although such numerical solvers exist for fixed and explicitly state-dependent advanced-retarded systems [13], there is no such software for implicitly state-dependent problems, such as we consider.

Since it is not possible to start from a linear approximation and use stability to converge to the periodic orbit of the full nonlinear system, we seek special values of the parameters for which the full nonlinear system has periodic orbits which correspond to the periodic orbits of the linearized system, and we find two classes of such solutions.

Figure 10 shows a periodic orbit of the full nonlinear system (1), (24) and (3)–(4) with the same masses $m_1$, $m_2$, separation $r_o$ and field ratio $\kappa$ as in the previous example. The only modification to the previous example is to set $\sigma = \pi$ in the linearized equations used to

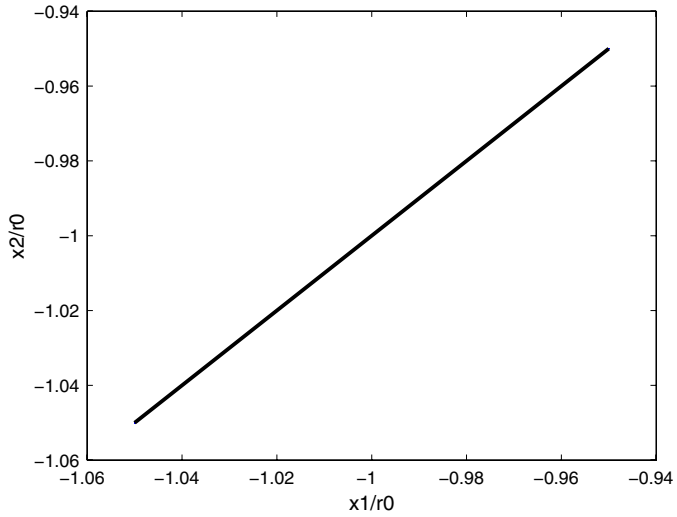


**Figure 10.** A periodic solution of period $T = 4004.625$ of the nonlinear system with $\chi = 0$, $m_1 = 1, m_2 = 2, r_o = 10^3, \varepsilon_o = 2.5 \times 10^{-7}, \kappa = 2$ and $\alpha = 9.8696 \times 10^3$ for which the linearized equations have $\sigma = \pi$ and $T_c = 4000$.

define the initial history which result in different values of $\alpha$ and $T_c$ at the bifurcation point. Figure 10 shows 250 periods of the solution of the full nonlinear equations with no apparent phase drift (compare to the drift seen in figure 7 over just 25 periods in the previous example). There is actually a whole family of such periodic solutions of the full nonlinear equations which we illustrate in figure 11 by showing the motion of particle 1 only (the motion of particle two is the same and in phase) for twenty such periodic orbits. This figure also shows that the amplitude of the oscillations remains constant. The numerical integration of the full nonlinear equations works in this case due to an extra symmetry introduced by the choice of $\sigma = \pi$. In this case the period of the zero amplitude solutions is $T = 4\pi r_o/\sigma = 4r_o$ which is twice the separation distance $2r_o$, so the advances and delays are exactly half a period, and fall on the same point in the periodic orbit for solutions of zero amplitude. In the full nonlinear system the period increases from $T = 4r_o = 4000$ (for the zero amplitude solutions) proportionally to the square of the amplitude of the solution (the largest orbit shown in figure 11 with a period of 4018.46).

In the two examples above, $\kappa$ is chosen to be equal to the ratio $m_2/m_1$, because this was found to result in motions where both particles oscillate with similar amplitudes. Other choices of $\kappa$ lead to the lighter particle having an amplitude of oscillation orders of magnitude larger than that of the heavier particle. This raises the question of whether we can choose parameter values which allow one particle to oscillate, while the other particle remains fixed in place, i.e. the frozen proton orbit. We now show that the linearized equations admit such solutions, and show numerically that they can persist for the full nonlinear equations.

Using the notation of (12), and recalling that $\chi = 0$ for the Wheeler–Feynman case, choosing parameters such that $B_- = 0$, $B_1 = 0$ and $B_2 \neq 0$ equation (11) is satisfied for $A_2 = 0$ and arbitrary values of $A_1$. In the notation of the previous section $B_- = 0$ and one of $B_i = 0$ implies that $\sigma \in \Sigma$ (while $\Sigma^*$ is the set of $\sigma$ such that $B_- = B_1 = B_2 = 0$). In numerical experiments we found that these orbits persist for the full nonlinear equations when the mass ratio $m_2/m_1$ and the separation $r_o$ are large. For small separations, or small

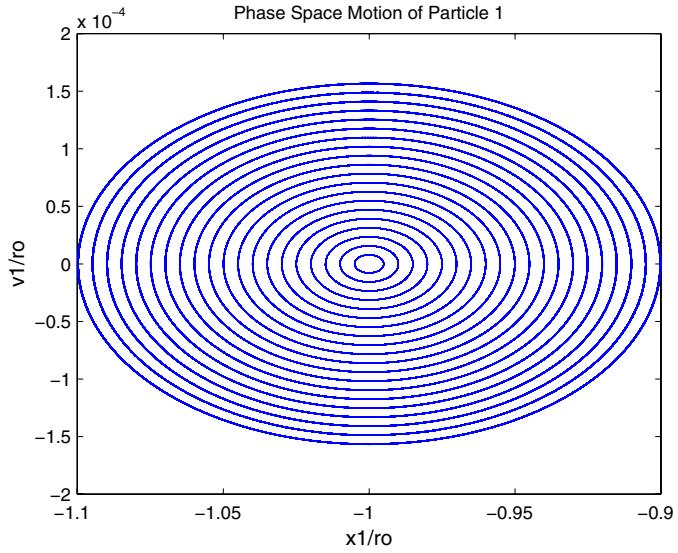


**Figure 11.** Periodic solutions of the nonlinear system with $\chi = 0$, $m_1 = 1$, $m_2 = 2$, $r_o = 10^3$, $\varepsilon_o = 2.5 \times 10^{-7}$, $\kappa = 2$, and $\alpha = 9.8696 \times 10^3$ for which the linearized equations have $\sigma = \pi$ and $T_c = 4000$, and the full nonlinear equations have periodic with period greater than 4000, with the period increasing with the amplitude. The motion of the first particle only is shown, and the smallest orbit shown has period $T = 4000.046\,28$ growing to $T = 4018.46$ for the largest orbit.

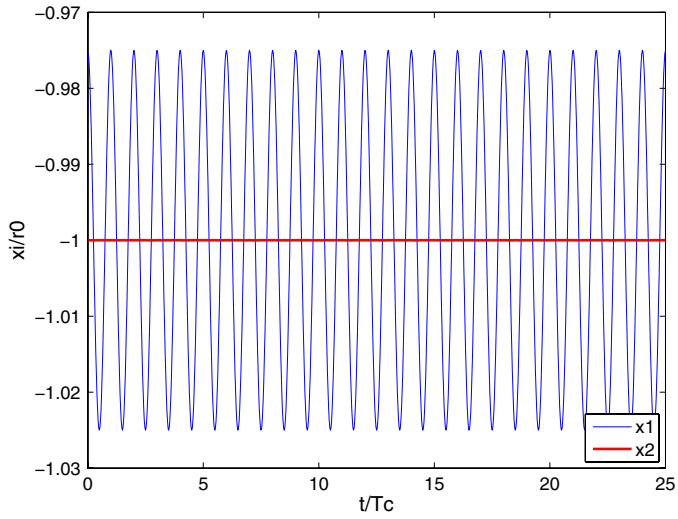


**Figure 12.** A periodic solution of the full nonlinear system with period $T = 4.491\,608 \times 10^5$ and $\chi = 0, m_1 = 1, m_2 = 1836, r_o = 10^5, \varepsilon_o = 2.5 \times 10^{-11}, \alpha_1 = 7.830\,97 \times 10^5\ \alpha_2 = 7.188\,25 \times 10^8$ for which the linearized equations have periodic orbits with particle 2 being stationary, and particle 1 performing periodic orbits of the form (31) about $-r_o$ of arbitrary amplitude with $\sigma = 2.798\,386$ and $T_c = 4.490\,578 \times 10^5$.

mass ratios, or when $B_2 \approx 0$, the heavily particle begins to oscillate with a small but growing amplitude.

In figure 12 we show such an orbit for the full nonlinear system with $m_2 = 1836$, $r_o = 10^5$ and $B_2 = \alpha_2 = (1 + m_2 r_o \sigma^2)/2$. The orbit is shown over 25 periods during which

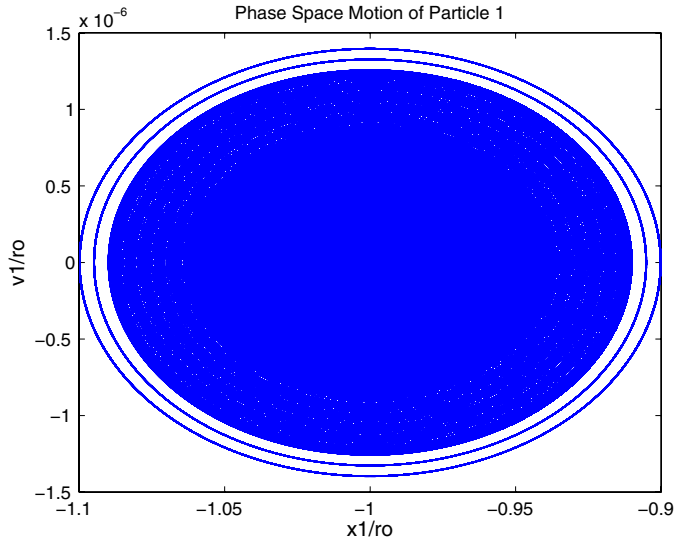


**Figure 13.** The motion of particle 1 for 20 periodic solutions of different amplitude and period for the nonlinear system with $\chi = 0$, $m_1 = 1$ , $m_2 = 1836$, $r_o = 10^5$, $\varepsilon_o = 2.5 \times 10^{-11}$, $\alpha_1 = 7.830\,97 \times 10^5$ $\alpha_2 = 7.18825 \times 10^8$ for which the linearized equations have $\sigma = 2.798\,386$ and $T_c = 4.490\,578 \times 10^5$, and the full nonlinear equations have a periodic orbits whose period increases with the amplitude of the solution (for the orbits shown $T$ varies between $4.490\,619 \times 10^5$ and $4.507\,037 \times 10^5$).

the heavy particle remains stationary to machine precision (the variation in $x_2$ over the whole time integration was $\pm 1.35 \times 10^{-17}$ from $-r_o$). In figure 13 we plot the motion of particle 1 only for the same orbit and 19 others, showing that there is a family of co-existing periodic orbits of this form. As in the previous example we find that the period of the nonlinear solutions increases from the critical period $T_c$ at zero amplitude, proportional to the square of the amplitude.

## 8. Conclusions and perspectives

In this paper, we have studied the electromagnetic two-body problem without introducing any approximation, i.e. keeping the state-dependent character of the interactions. By using a surrogate dynamical system, making use of the periodicity to convert advances to delays or vice versa, and in the case of the Dirac model integrating backward in time, and using appropriate software [10], we are able to determine periodic solutions for the equations of motion of two particles moving along the same straight line. This setup, besides providing a testbed for the algorithms to handle equations with state-dependent delay, revealed some of the subtleties of the Lorentz–Dirac equations, confirming that qualitative differences arise when both particle masses are finite. For the Dirac case we showed that no bifurcation can occur at the physical fixed point. For the unphysical point we found a bifurcating orbit of the Dirac-like case, which served as an example of state-dependent delay dynamics with electromagnetic-like difficulties. We determined a subcritical Hopf bifurcation for the surrogate equations of motion and thus for the Dirac-like equations near the unphysical point. The linear stability analysis also guided the search for periodic orbits for the Wheeler–Feynman case, and we found several interesting families of periodic orbits of physical interest. The bifurcation

structure of the fixed point in the Wheeler–Feynman case could not be accessed because of the time-reversibility of the system. The frozen-particle orbit could be expected in this setup given the linear dependence of the electrostatic external field at each particle. In a three-dimensional setup the external force is not needed for a bounded orbit, as the attraction can provide the centripetal force for rotation. The analog of a frozen-particle orbit for a three-dimensional case without external field should be interesting. Given the peculiarity of the 1D case, it would certainly be interesting to pass to the more realistic and physical case of a 2D/3D setup. A linearized version of such a case is considered in [15]. Our method might be generalizable to find periodic orbits of electromagnetic motion in three spatial dimensions, but unfortunately, apart from the one-dimensional motion, the Wheeler–Feynman equations are neutral-delay equations. For such equations solution derivatives can be discontinuous and there may be solution termination [16], while periodic orbits with a discontinuous acceleration at breaking points could exist [14]. Furthermore, an even less intuitive two-body dynamics could be found for larger velocities (close to the speed of light) [14], but in order to simulate these, it would be necessary to handle the stiffness of the electromagnetic equations of motion. The bifurcation analysis of the Wheeler–Feynman case, as well as a proper determination of the frozen proton orbit, await the construction of a boundary-value problem solver for implicitly state-dependent problems.

## Acknowledgments

The authors acknowledge discussions with Giorgio Fusco, Ernst Hairer, Antonio Ponno, Bob Rink, Hildebrando Rodrigues and Savio B Rodrigues. This work was partially supported by CNPQ (Brazil), FAPESP (Brazil), GNCS INDAM (Italy) and NSERC (Canada).

## References

[1] Aiello W G, Freedman H I and Wu J 1992 *SIAM J. Appl. Math.* **52** 885
[2] Mohanty P K and Politi A 2006 *J. Phys. A: Math. Gen.* **39** L415
[3] Kye W-H, Choi M, Kim M-W, Lee S-Y, Rim S, Kim C-M and Park Y-J 2004 *Phys. Rev.* E **69** 055202(R)
[4] Eliezer C J 1947 *Rev. Mod. Phys.* **19** 147
[5] Dirac P A M 1938 *Proc. R. Soc.* A **167** 148
[6] Eliezer C J 1943 *Proc. Camb. Phil. Soc.* **39** 173
[7] De Luca J 2006 *Phys. Rev.* E **73** 026221
[8] Wheeler J A and Feynman R P 1945 *Rev. Mod. Phys.* **17** 157
Wheeler J A and Feynman R P 1949 *Rev. Mod. Phys.* **21** 425
[9] Huschilt J and Baylis W E 1976 *Phys. Rev.* D **13** 3256
Huschilt J and Baylis W E 1978 *Phys. Rev.* D **17** 985
[10] Guglielmi N and Hairer E 2001 *Computing* **67** 1
Guglielmi N and Hairer E 2008 *Adv. Comput. Math* **29** 229
[11] De Luca J 2007 *J. Math. Phys.* **48** 012702
[12] Schild A 1963 *Phys. Rev.* **131** 2762
[13] Abell K A, Elmer C E, Humphries A R and Van Vleck E S 2005 *SIAM J. Appl. Dyn. Syst.* **4** 755
[14] De Luca J 2009 *J. Math. Phys.* **50** 062701
[15] Marino M, Carati A and Galgani L 2007 *Ann. Phys.* **322** 799
[16] Bellen A, Guglielmi N, Maset S and Zennaro M 2009 *Acta Numer.* **18** 1